Proceedings of the
National Academy of Sciences
of the United States of America

RESEARCH ARTICLE

Duration of urination does not change with body size

Patricia J. Yang, Jonathan Pham, Jerome Choo, and David L. Hu
+ See all authors and affiliations

PNAS August 19, 2014 111 (33) 11932-11937; first published June 26, 2014; https://doi.org/10.1073/pnas.1402289111

Edited by David A. Weitz, Harvard University, Cambridge, MA, and approved May 14, 2014 (received for review February 6, 2014)

Significance

Animals eject fluids for waste elimination, communication, and defense from predators. These diverse systems all rely on the fundamental principles of fluid mechanics, which we use to predict urination duration across a wide range of mammals. In this study, we report a mathematical model that clarifies misconceptions in urology and unifies the results from 41 independent urological and anatomical studies. The theoretical framework presented may be extended to study fluid ejection from animals, a universal phenomenon that has received little attention.

Abstract

Many urological studies rely on models of animals, such as rats and pigs, but their relation to the human urinary system is poorly understood. Here, we elucidate the hydrodynamics of urination across five orders of magnitude in body mass. Using high-speed videography and flow-rate measurement obtained at Zoo Atlanta, we discover that all mammals above 3 kg in weight empty their bladders over nearly constant duration of 21 ± 13 s. This feat is possible, because larger animals have longer urethras and thus, higher gravitational force and higher flow speed. Smaller mammals are challenged during urination by high viscous and capillary forces that limit their urine to single drops. Our findings reveal that the urethra is a flow-enhancing device, enabling the urinary system to be scaled up by a factor of 3,600 in volume without compromising its function. This study may help to diagnose urinary problems in animals as well as inspire the design of scalable hydrodynamic systems based on those in nature.

urology allometry scaling Bernoulli's principle

Medical and veterinary urology often relies on simple, noninvasive methods to characterize the health of the urinary system (**1**, **2**). One of the most easily measured characteristics of the urinary system is its flow rate (**3**), changes in which may be used to diagnose urinary problems. The expanding prostates of aging males may constrict the urethra, decreasing urine flow rate (**4**). Obesity may increase abdominal pressure, causing incontinence (**5**). Studies of these ailments and others often involve animal subjects of a range of sizes (**6**). A study of urination in zero gravity involved a rat suspended on two legs for long periods of time (**7**), whereas other studies involve mice (**8**), dogs (**1**), and pigs (**9**). Despite the wide range of animals used in urological studies, the consequences of body size on urination remain poorly understood.

The bladder serves a number of functions, as reviewed by Bentley (**10**). In desert animals, the bladder stores water to be retrieved at a time of need. In mammals, the bladder acts as a waterproof reservoir to be emptied at a time of convenience. This control of urine enables animals to keep their homes sanitary and themselves inconspicuous to predators. Stored urine may even be used in defense, which one knows from handling rodents and pets.

Several misconceptions in urology have important repercussions in the interpretation of healthy bladder function. For instance, several investigators state that urinary flow is driven entirely by bladder pressure. Consequently, their modeling of the bladder neglects gravitational forces (**11⇓–13**). Others, such as Martin and Hillman (**14**), contend that urinary flow is driven by a combination of both gravity and bladder pressure. In this study, we elucidate the hydrodynamics of urination across animal size, showing the effects of gravity increase with increasing body size.

Results

In Vivo Experiments.

We filmed the urination of 16 animals and obtained 28 videos of urination from YouTube, listed in *SI Appendix*. Movies S1–S4 show that urination style is strongly dependent on animal size. Here, we define an animal as large if it is heavier than 3 kg and an animal as small if it is lighter than 1 kg. Large animals, from dogs to elephants, produce jets and sheets of urine, which are shown in **Fig. 1 *A–D***. Small animals, including rodents, bats, and juveniles of many mammalian species, cannot generate jets. Instead, they urinate using a series of drops, which is shown by the 0.03-kg lesser dog-faced fruit bat and the 0.3-kg rat in **Fig. 2 *A–C***, respectively.

Continue

Fig. 1.

Download figure | Open in new tab | Download powerpoint

Jetting urination by large animals, including (*A*) elephant, (*B*) cow, (*C*) goat, and (*D*) dog. *Inset* of cow is reprinted from the public domain and cited in *SI Appendix*. (*E*) Schematic of the urinary system. (*F*) Ultrasound image of the bladder and urethra of a female human. The straight arrow indicates the urethra, and the curved arrow indicates the bladder. Reproduced with permission from ref. **20**, (Copyright 2005, Radiological Society of North America). (*G*) Transverse histological sections of the urethra from a female pig. Reproduced with permission from ref. **9**, (Copyright 2001, Elsevier). (*H*) The relationship between body mass and urination time.

Fig. 2.

Download figu Continue w tab | Download powerpoint

Dripping urination by small animals. (*A*) A rat's excreted urine drop. (*B*) A urine drop released by the lesser dog-faced fruit bat *Cynopterus brachyotis*. Courtesy of Kenny Breuer and Sharon Swartz. (*C*) A rat's urine drop grows with time. *Inset* is reprinted from the public domain and cited in *SI Appendix*. (*D*) Time course of the drop radii of the rat (triangles) along with prediction from our model (blue dotted line, $\alpha = 0.5$; green solid line, $\alpha = 1$; red dashed line, $\alpha = 0.2$).

Movie S1.

Open in new tab | Download original movie

Movie S1. Urination of a rat (mass of 0.24 kg). Time slowed by 33 times.

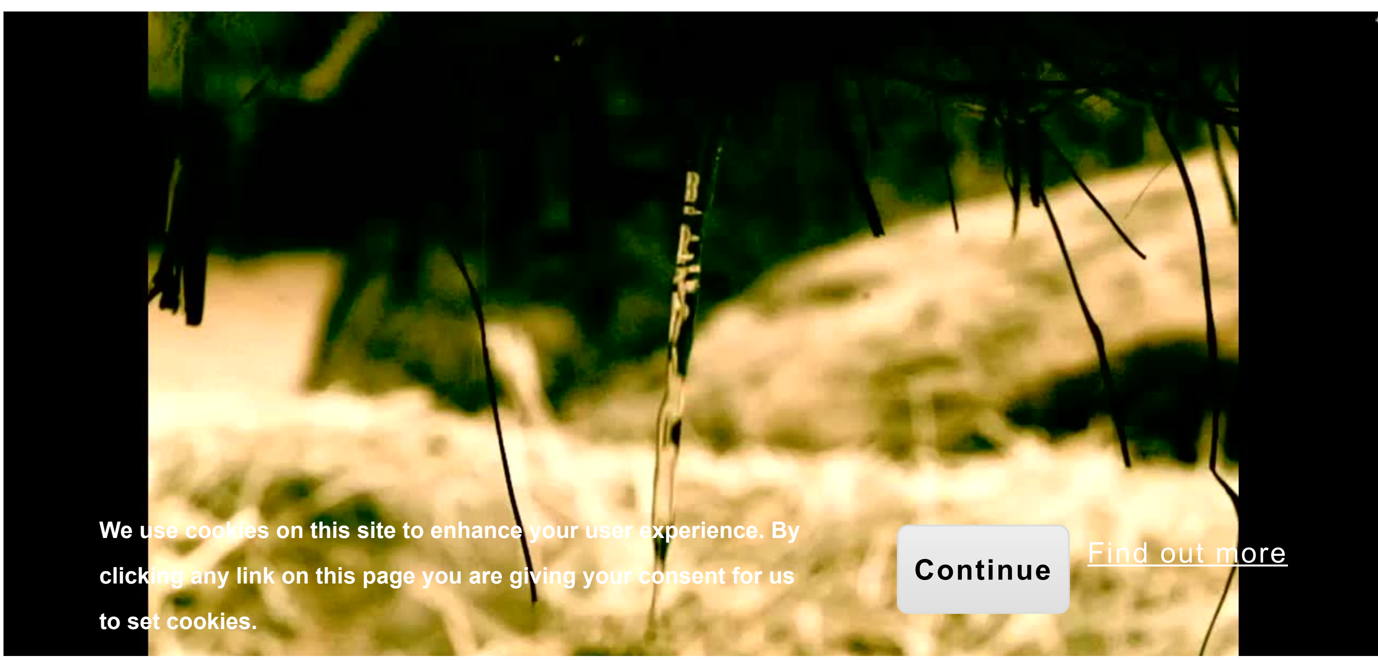

Movie S2.

Open in new tab | **Download original movie**

Movie S2. Urination of a goat (mass of 70 kg). Time slowed by 17 times.

Movie S3.

Open in new tab | **Download original movie**

Movie S3. Urination of a cow (mass of 640 kg). Time slowed by 33 times.

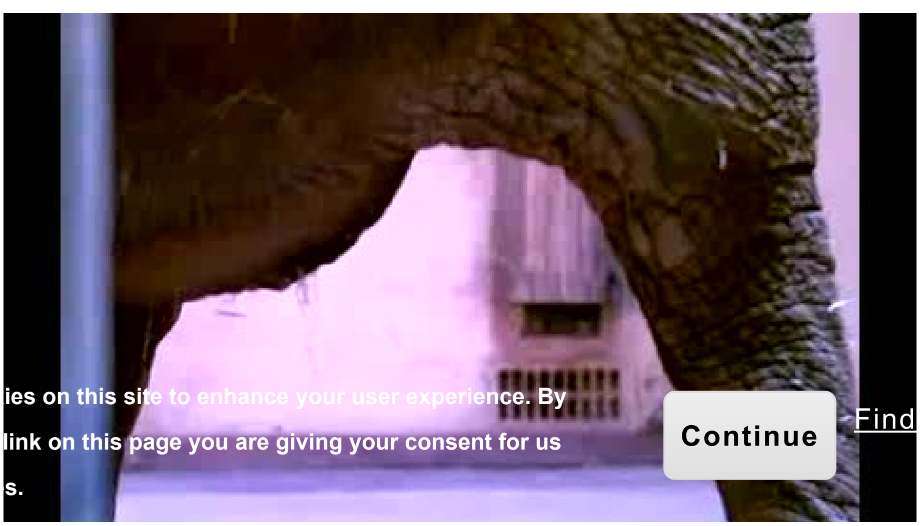

Movie S4.

Movie S4. Urination of an elephant (mass of 3,540 kg). Time slowed by 33 times.

Fig. 1*H* shows the urination time for 32 animals across six orders of magnitude of body mass from 0.03 to 8,000 kg. Despite this wide range in mass, urination time remains constant, $T = 21 \pm 13$ s ($n = 32$), for all animals heavier than 3 kg. This invariance is noteworthy, considering that an elephant's bladder, at 18 L, is nearly 3,600 times larger in volume than a cat's bladder at 5 mL. Using the method of least squares, we fit the data to a clear scaling law shown by the dashed line: $T \sim M^{0.13}$ (**Fig. 1*H***).

For small animals, urination is a high-speed event of 0.01- to 2-s duration and therefore, quite different from the behavior of the large animals observed that urinate for 21 s. **Fig. 1*H*** shows urination time across 11 small animals, including one bat, five rats, and five mice. Their body masses ranged from 0.03 to 0.3 kg. The large error bar for the rats is caused by bladder fullness varying across individuals. **Fig. 2*D*** shows the time course of the urine drop's radius measured by image analysis of high-speed video of a rat. To rationalize the striking differences between large and small animals, we turn to mathematical modeling of the urinary system.

Modeling Assumptions.

Urination may be simply described mathematically. **Fig. 1*E*** shows a schematic of the urinary system, consisting of a bladder of volume V and the urethra, which is assumed to be a straight vertical pipe of length L and diameter D. We assume that the urethra has such a thin wall that its internal and external diameters are equal. Urination begins when the smooth muscles of the bladder pressurize the urine to $P_{bladder}$, measured relative to atmospheric pressure. After an initial transient of duration that depends on the system size, a steady flow of speed u is generated.

Previous medical and veterinary studies, particularly cystometrography and ultrasonography, report substantial data on the anatomy, pressure, and flow rate of the urinary system. **Fig. 3** shows urethral length (**8**, **15⇓⇓⇓⇓⇓⇓⇓⇓⇓–25**) and diameter (**15**, **24⇓⇓⇓⇓⇓⇓⇓⇓⇓–34**), flow rate (**35⇓⇓⇓⇓⇓⇓–42**), bladder capacity (**25**, **43⇓⇓⇓⇓⇓–49**), and bladder pressure (**1**, **35**, **39**, **40**, **43**, **46**, **50**) for over 100 individuals across 13 species. **Table 1** shows the corresponding allometric relationships to be used in numerical predictions for flow rate and urination time.

Fig. 3.

Download figure | Open in new tab | Download powerpoint

The relation between body mass *M* and properties of the urinary system. (*A*) Urethral length *L* (green triangles) and diameter *D* (blue circles). (*B*) Bladder capacity *V*. (*C*) Shape factor *α* associated with the urethral cross-section. (*D*) Bladder pressure $P_{bladder}$. (*E*) Flow rate of males. (*F*) Flow rate of females. Symbols represent experimental measurements, dashed lines represent best fits to the data, and solid lines represent predictions from our model.

Table 1.

VIEW INLINE | VIEW POPUP

Measured allometric relationships for the urinary system of animals

We begin by showing that the urinary system is isometric (i.e., it has constant proportions across animal size). **Fig. 3*A*** shows the relation between body mass *M* and urethral dimensions (length *L* and diameter *D*). As shown by the nearly parallel trends for *L* and *D* ($L = 35M^{0.43}$ and $D = 2M^{0.39}$), the aspect ratio of the urethra is 18. Moreover, the exponents are close to the expected isometric scaling of $M^{1/3}$. **Fig. 3*B*** shows the relationship between body mass and bladder capacity. The bladder's capacity is $V \sim M^{0.97}$, and the exponent of near unity indicates isometry.

In ultrasonic imaging (**Fig. 1*F***), the urethra appears circular (**20**). However, in histology (**Fig. 1*G***), the urethra is clearly corrugated, which decreases its cross-sectional area (**9**). The presence of such corrugation has been verified in studies in which flow is driven through the urethra (**51**, **52**), although the precise shape has been too difficult to measure. We proceed by using image analysis to measure cross-sectional area *A* from urethral histological diagrams of dead animals in the absence of flow (**9**, **53**, **54**). We define a shape factor $\alpha = 4A/\pi D^2$, which relates the urethral cross-sectional area with respect to that of a cylinder of diameter *D*. **Fig. 3*C*** shows the shape factor $\alpha = 0.2 \pm 0.05$ ($n = 5$) for which the corrected cross-sectional area is 20% of the original area considered. This shape factor is nearly constant across species and body mass and consistent with the value of 0.17 found by Wheeler et al. (**55**).

Peak bladder pressure is difficult to measure in vivo, and instead, it is estimated using pressure transducers placed within the bladders of anesthetized animals. Pressure is measured when the bladder is filled to capacity by the injection of fluid. This technique yields a nearly constant bladder pressure across animal size: P_{bladder} = 5.2 ± 0.86 kPa (n = 8), which is shown in **Fig. 3*D***. The constancy of bladder pressure at 5.2 kPa is consistent with other systems in the body. One prominent example is the respiratory system, which generates pressures of 10 kPa for animals spanning from a mosquito to an elephant (**56**).

Steady-State Equation of Urine Flow.

We model the flow as steady state and the urine as an incompressible fluid of density ρ, viscosity μ, and surface tension σ. The energy equation relates the pressures involved, each of which has units of energy per cross-sectional area of the urethra per unit length down the urethra:

$$P_{\text{bladder}} + P_{\text{gravity}} = P_{\text{inertia}} + P_{\text{viscosity}} + P_{\text{capillary}}. \tag{1}$$

Each term in **Eq. 1** may be written simply by considering the pressure difference between the entrance and exit of the urethra. The combination of bladder and hydrostatic pressure drives urine flow. Bladder pressure P_{bladder} is a constant given in **Fig. 3*D***. We do not model the time-varying height in the bladder, because bladders vary greatly in shape (**57**). Thus, hydrostatic pressure scales with urethral length: $P_{\text{gravity}} \sim \rho g L$, where g is the acceleration of gravity. Dynamic pressure P_{inertia} scales as $\rho u^2/2$ and is associated with the inertia of the flow.

The viscous pressure drop in a long cylindrical pipe is given by the Darcy–Weisbach equation (**58**): $P_{\text{viscosity}} = f_D(\text{Re})\rho L u^2/2\alpha D$. We use $\sqrt{\alpha}D$ as the effective diameter of the pipe to keep the cross-sectional area of the pipe consistent with experiments. The Darcy friction factor f_D is a function of the Reynolds number Re = $\rho u D/\mu$, such that $f_D(\text{Re}) = 64/\text{Re}$ for laminar flow and $f_D(\text{Re}) = 0.316/\text{Re}^{1/4}$ for turbulent flow ($10^4 < \text{Re} < 10^5$). Drops generated from an orifice of effective diameter $\sqrt{\alpha}D$ experience a capillary force (**59**) of $P_{\text{capillary}} = 4\sigma/\sqrt{\alpha}D$. Substituting these terms into **Eq. 1**, we arrive at

$$P_{\text{bladder}} + \rho g L = \frac{\rho u^2}{2} + f_D(\text{Re})\frac{\rho L u^2}{2\alpha D} + \frac{4\sigma}{\sqrt{\alpha}D}. \tag{2}$$

The relative magnitudes of the five pressures enumerated in **Eq. 2** are prescribed by six dimensionless groups, including the aforementioned Reynolds number and Darcy friction factor and well-known Froude $\text{Fr} = u/\sqrt{gL}$ and Bond Bo = $\rho g D^2/\sigma$ numbers (**60**) as well as dimensionless groups pertaining to the urinary system, the urethra aspect ratio As = D/L, and pressure ratio Pb = $P_{\text{bladder}}/\rho g L$. Using these definitions, we nondimensionalize **Eq. 2** to arrive at

$$\text{Pb} + 1 = \frac{\text{Fr}^2}{2} + f_D(\text{Re})\frac{\text{Fr}^2}{2\alpha\text{As}} + \frac{4\text{As}}{\sqrt{\alpha}\text{Bo}}. \tag{3}$$

In the following sections, we solve **Eq. 3** in the limits of large and small

In *SI Appendix*, we apply a variation of the Washburn law (**61**) to show that the steady-state model given in **Eq. 2** is accurate for most animals. Animals lighter than 100 kg achieve 90% of their flow velocity within 4 s; however, for animals such as elephants, the transient phase can be substantial. For our derivations here, however, we assume that the transient phase is negligible.

Large Animals Urinate for Constant Duration.

Bladder pressure, gravity, and inertia are dominant for large animals, which can be shown by consideration of the dimensionless groups in *SI Appendix*. **Eq. 2** reduces to

$$P_{\mathrm{bladder}} + \rho g L = \frac{\rho u^2}{2}. \tag{4}$$

The urination time T, the time to completely empty the bladder, may be written as the ratio of bladder capacity to time-averaged flow rate, $T = V/Q$. We define the flow rate as $Q = uA$, where $A = \alpha\pi D^2/4$ is the cross-sectional area of the urethra. Using **Eq. 4** to substitute for flow speed yields

$$T = \frac{4V}{\alpha\pi D^2\left(\frac{2P_{\mathrm{bladder}}}{\rho} + 2gL\right)^{1/2}}. \tag{5}$$

By isometry, bladder capacity $V \sim M$ and urethral length and diameter both scale with $M^{1/3}$; substitution of these scalings into **Eq. 5** yields urination time $T \sim M^{1/6} \approx M^{0.16}$ in the limit of increasing body mass. Agreement between predicted and measured scaling exponents is very good (0.13 compared with 0.16). We, thus, conclude that our scaling has captured the observed invariance in urination time.

We go beyond a simple scaling by substituting the measured allometric relationships from **Table 1** for L, D, α, V, and P_{bladder} into **Eq. 5**, yielding a numerical prediction for urination time. This prediction (**Fig. 1*H***, solid line) is shown compared with experimental values (**Fig. 1*H***, dashed line). The general trend is captured quite well. We note that numerical values are underpredicted by a factor of three across animal masses, likely because of the angle and cross-section of the urethra in vivo.

How can an elephant empty its bladder as quickly as a cat? Larger animals have longer urethras and therefore, greater hydrostatic pressure driving flow. Greater pressures lead to higher flow rates, enabling the substantial bladders of larger animals to be emptied in the same duration as those of their much smaller counterparts.

Our model provides a consistent physical picture on consideration of flow rate. Combining **Eq. 4** and the definition of flow rate ($Q = uA$) yields

$$Q = \frac{\alpha\pi D^2}{4}\left(\frac{2P_{\mathrm{bladder}}}{\rho} + 2gL\right)^{1/2}. \tag{6}$$

Continue

Our model gives insight into the distinct flow-rate scalings observed for both male and female mammals. Male mammals generally stand on four legs and have a penis that extends downward, enabling them to urinate vertically. Assuming isometry ($D \sim M^{1/3}$ and $L \sim M^{1/3}$), flow rate scales as $Q \sim M^{5/6} \approx M^{0.83}$ in the limit of large body mass. This predicted exponent is within 10% of the observed scaling for males: $Q_M \sim M^{0.92}$. By substituting the allometric relations from **Table 1** into **Eq. 6**, we compute a numerical prediction for flow rate (**Fig. 3*E***, solid line) that is five times higher than experimental flow rates (**Fig. 3*E***, dashed line). This overprediction is roughly consistent with our underprediction for urination time.

Female mammals have anatomy such that the urethral exit is near the anus: thus, many female animals urinate horizontally. The scaling of **Eq. 6** without the gravitational term is $Q \sim M^{2/3} \approx M^{0.67}$, and the exponent is in correspondence to that found in our experiments for females: $Q_F \sim M^{0.66}$. Substituting allometric relations from **Table 1** yields a numerical prediction (**Fig. 3*F***, solid line) that remains in good agreement with experiments.

Small Animals Urinate Quickly and for Constant Duration.

Bladder pressure, viscous pressure, and capillary pressure are dominant for small animals, which is shown by the associated dimensionless groups in *SI Appendix*. In this limit, **Eq. 2** reduces to

$$P_{\text{bladder}} = \frac{\rho u^2}{2} + \frac{32\mu L u}{\alpha D^2} + \frac{4\sigma}{\sqrt{\alpha}D}, \tag{7}$$

which we solve numerically for flow speed u. To predict the flow speed of a rat, inputs to this equation include the rat's bladder pressures and urethral anatomy (**15**, **16**, **50**) (P_{bladder} = 6.03 kPa, L = 20 mm, D = 0.8 mm).

To determine urination time, we turn to the dynamics of drop filling. A spherical drop is filled by the influx of urine, $Q = \alpha\pi D^2 u/4$. By conservation of mass, $dV_{\text{drop}}/dt = Q$, a first-order differential equation that may be easily integrated to obtain the drop volume $V(t)$. We assume that the initial drop corresponds to a sphere of the same diameter as the urethra, $\sqrt{\alpha}D$. Thus, the radius of the spherical urine drop may be written

$$R(t) = \left(\frac{\alpha^{\frac{3}{2}} D^3}{8} + \frac{3\alpha D^2 u t}{16}\right)^{1/3}. \tag{8}$$

Combining **Eq. 8** and the numerical solution for **Eq. 7**, we compute the time course of the drop radius. This prediction is compared with experimental values in **Fig. 2*D***. We find that the prediction is highly sensitive to the value of α. Without consideration of the corrugated cross-section, a prediction of $\alpha = 1$ (**Fig. 2*D***, green solid line) yields a flow rate that is too high. Using the shape factor $\alpha = 0.2$ (**Fig. 2*D***, red dashed line), our model predicts a flow speed of u = 1.2 m/s, which fits the data fairly well. Using nonlinear least-squares fitting in Matlab, the best fit to the experimental data yields an intermediate value of $\alpha = 0.5$ (**Fig. 2*D***, blue dotted line).

Continue

The drop does not grow without limit but falls when its gravitational force, scaling as $4\pi R_f^3 \rho g/3$, overcomes its attaching capillary force to the urethra, scaling as $\pi\sqrt{\alpha}\,D\sigma$. Equating these two forces yields the final drop radius before detachment,

$$R_f = \left(\frac{3\sigma\sqrt{\alpha}\,D}{4\rho g}\right)^{1/3}, \tag{9}$$

which does a fair job of predicting the drop size. We predict drop radii for rats and mice of 1.3 and 1.1 mm, respectively, which are two times as large as experimental values of 2.0 ± 0.1 (n = 5) and 2.2 ± 0.4 mm (n = 5), respectively. We suspect this difference is caused by our underestimation of urethral perimeter at the exit. For such a large drop to remain attached, we require the attachment diameter to be larger by a factor of two, which is quite possible, because the urethral exit is elliptical.

Substituting **Eq. 9** into **Eq. 8**, the time to eject one drop may be written

$$T_{\text{drop}} = \frac{16\sqrt{\alpha}\,D}{3u}\left(\frac{3\cos\theta}{4\alpha^{\frac{3}{2}}\,\text{Bo}} - \frac{1}{8}\right) \approx \frac{4\,D\cos\theta}{\sqrt{\alpha}\text{Bo}}\,\frac{1}{u}. \tag{10}$$

The predictions of maximum drop size and time to fall are in excellent correspondence with observed values for rats and mice. Using **Eq. 10**, we predict drop falling times of 0.05 and 0.15 s for rats and mice, respectively, which are nearly identical to experimental values of 0.06 ± 0.05 (n = 5) and 0.14 ± 0.1 s (n = 14), respectively.

A scaling for urine duration for small animals is not straightforward because of the nonlinearity of **Eq. 7**. We conduct a scaling analysis in the limit of decreasing animal size for which the Reynolds number approaches zero. Because of isometry, $V \sim M$ and $D \sim M^{1/3}$. Rewriting **Eq. 7** at low Reynolds number, we have $u \sim D$, and therefore, the time to eject one drop from **Eq. 10** scales as $T_{\text{drop}} \sim \text{Bo}^{-1} \sim M^{-2/3}$. Using **Eq. 9**, the final drop size is $R_f \sim D \sim M^{1/3}$. By conservation of mass, a full bladder of volume V can produce N spherical drops, where $N = 3V/4\pi R_f^3 \sim M^{2/3}$. Thus, the urination time for small animals $T = NT_{\text{drop}}$ is constant and therefore, independent of animal size. This prediction indicates that small animals urinate for different durations than large animals, which is in correspondence with experiments. Our experiments indicate that mammals of mass 0.03–0.3 kg urinate for durations of 0.1–2 s. We have insufficient range of masses for small animals to conclude our prediction that urination time is constant in this regime.

The model yields insight into the challenges faced by small animals. In **Eq. 7**, flow speed is positive only if $P_{\text{bladder}}\sqrt{\alpha}\,D \geq 4\sigma$, where σ is the surface tension of urine, which for humans is comparable with the surface tension of water (**62**). Thus, we predict that the smallest urethra to expel urine has a diameter of $4\sigma/\sqrt{\alpha}\,P_{\text{bladder}} \sim 0.1\ \text{mm}$. According to our allometric trends, the smallest animal that can urinate independently corresponds to a body mass of 0.8 g and urethral length of 1.7 mm. This mass corresponds to that of altricial mice (0.5–3 g), which are dependent on their mother's lic[illegible]ted urine drops (**63**).

Discussion

The urinary system works effectively across a range of length scales. This robustness is caused by the hydrodynamic contribution of the urethra. In the medical literature, the function of the urethra was previously unknown. It was simply defined as a conduit between bladder and genitals. In this study, we find that the urethra is analogous to Pascal's Barrel: by providing a water-tight pipe to direct urine downward, the urethra increases the gravitational force acting on urine and therefore, the rate at which urine is expelled from the body. Thus, the urethra is critical to the bladder's ability to empty quickly as the system is scaled up. Engineers may apply this result to design a system of pipes and reservoirs for which the drainage time does not depend on system size. This concept of a scalable hydrodynamic system may be used in the design of portable reservoirs, such as water towers, water backpacks, and storage tanks.

Why is urination time 21 s, and why is this time constant across animal sizes? The numerical value of 21 s arises from the underlying physics involving the physical properties of urine as well as the dimensions of the urinary system. Our model shows that differences in bladder capacity are offset by differences in flow rate, resulting in a bladder emptying time that does not change with system size. Such invariance has been observed in a number of other systems. Examples include the height of a jump (**64**) and the number of heartbeats in a lifetime (**65**). Many of these examples arise from some aspect of isometry, such as with our system.

From a biological perspective, the invariance of urination time suggests its low functional significance. Because bladder volume is 4.6 mL/kg body mass and daily urine voided is 26 mL/kg body mass (**66**), mammals urinate 5.6 times/d. Because the time to urinate once is 21 s, the daily urination time is 2 min, which can be translated to 0.2% of an animal's day, a negligible portion compared with other daily activities, such as eating and sleeping, for which most animals take care to avoid predation. Thus, urination time likely does not influence animal fitness. The geometry of the urethra, however, may play a role in other activities of high functional significance, such as ejaculation.

In our study, we found that urination time is highly sensitive to urethral cross-section. This dependency is particularly high for small animals for which urine flow is resisted by capillary and viscous forces, which scale with the perimeter of the urethra. More accurate predictions for small animals require measurements of the urethral exit perimeter and the urethral cross-section, which is known to vary with distance down the urethra (**67**). Current models of noncircular pipe flow are not applicable, because they only account for infinitesimal corrugations (**68**). Additional mathematical techniques as well as accurate urethral measurements are needed to increase correspondence with experiments.

Materials and Methods

We filmed urination of animals using both Sony HDR-XR200 and high-speed cameras (Vision Research v210 and Miro 4). The masses of animals are taken from annual veterinary procedures or measured using an analytical balance. Flow rate Q is measured by simultaneous high-spee y and manual urine collection using containers of appropriate size and shape. We use the open-source software Tracker to measure the time course of the radius of urine drops produced by rats and mice.

Acknowledgments

We acknowledge photographer C. Hobbs and our hosts at Zoo Atlanta (R. Snyder), the University of Georgia (L. Elly), the Atlanta Humane Society (A. Lopez), and the animal facilities at Georgia Tech (L. O'Farrell). We thank YouTube contributors, including Alex Cobb, Cole Onyx, demondragon115, drakar2835, ElMachoPrieto83, Ilze Darguže, Joe BERGMANN, Joey Ponticello, krazyboy35, laupuihang, MegaTobi89, Mixetc, mpwhat, MrTitanReign, relacsed, RGarrido121, ronshausen63, Sandro Puelles, Silvia Lugli, and Tom Holloway. Our funding sources were National Science Foundation Faculty Early Career Development Program (Division of Physics) Grant 1255127 for the modeling and Georgia Tech President's Undergraduate Research Awards for the experiments.

Footnotes

↵ [1]To whom correspondence should be addressed. Email: hu@me.gatech.edu.

Author contributions: P.J.Y. and D.L.H. designed research; J.P. and J.C. performed research; P.J.Y. and D.L.H. analyzed data; and P.J.Y. and D.L.H. wrote the paper.

The authors declare no conflict of interest.

This article is a PNAS Direct Submission.

This article contains supporting information online at www.pnas.org/lookup/suppl/doi:10.1073/pnas.1402289111/-/DCSupplemental.

References

1. ↵ Hinman F (1971) *Hydrodynamics of Micturition* (Thomas, New York). . Google Scholar
2. ↵ Griffiths DJ (1973) The mechanics of the urethra and of micturition. *Br J Urol* **45**(5):497–507. . CrossRef PubMed Google Scholar
3. ↵ Schäfer W, et al., International Continence Society (2002) Good urodynamic practices: Uroflowmetry, filling cystometry, and pressure-flow studies. *Neurourol Urodyn* **21**(3):261–274. . CrossRef PubMed Google Scholar
4. ↵ Girman CJ, et al. (1995) Natural history of prostatism: Relationship among symptoms, prostate volume and peak urinary flow rate. *J Urol* **153**(5):1510–1515. . CrossRef PubMed Google Scholar

5. ↵ Dwyer PL, Lee ET, Hay DM (1988) Obesity and urinary incontinence in women. *Br J Obstet Gynaecol* **95**(1):91–96. . CrossRef PubMed Google Scholar

6. ↵ Sibley GN (1984) A comparison of spontaneous and nerve-mediated activity in bladder muscle from man, pig and rabbit. *J Physiol* **354**:431–443. . Abstract/FREE Full Text Google Scholar

7. ↵ Ortiz RM, Wang TJ, Wade CE (1999) Influence of centrifugation and hindlimb suspension on testosterone and corticosterone excretion in rats. *Aviat Space Environ Med* **70**(5):499–504. . PubMed Google Scholar

8. ↵ St Clair MB, Sowers AL, Davis JA, Rhodes LL (1999) Urinary bladder catheterization of female mice and rats. *Contemp Top Lab Anim Sci* **38**(3):78–79. . PubMed Google Scholar

9. ↵ Dass N, McMurray G, Greenland JE, Brading AF (2001) Morphological aspects of the female pig bladder neck and urethra: Quantitative analysis using computer assisted 3-dimensional reconstructions. *J Urol* **165**(4):1294–1299. . CrossRef PubMed Google Scholar

10. ↵ Bentley PJ (1979) The vertebrate urinary bladder: Osmoregulatory and other uses. *Yale J Biol Med* **52**(6):563–568. . PubMed Google Scholar

11. ↵ Rao SG, Walter JS, Jamnia A, Wheeler JS, Damaser MS (2003) Predicting urethral area from video-urodynamics in women with voiding dysfunction. *Neurourol Urodyn* **22**(4):277–283. . CrossRef PubMed Google Scholar

12. ↵ Walter JS, Wheeler JS, Morgan C, Plishka M (1993) Urodynamic evaluation of urethral opening area in females with stress incontinence. *Int Urogynecol J* **4**(6):335–341. . CrossRef Google Scholar

13. ↵ Barnea O, Gillon G (2001) Model-based estimation of male urethral resistance and elasticity using pressure-flow data. *Comput Biol Med* **31**(1):27–40. . CrossRef PubMed Google Scholar

14. ↵ Martin JA, Hillman SS (2009) The physical movement of urine from the kidneys to the urinary bladder and bladder compliance in two anurans. *Physiol Biochem Zool* **82**(2):163–169. . CrossRef PubMed Google Scholar

15. ↵ Chang S, Chern I, Bown SG (2000) Photodynamic therapy of rat bladder and urethra: Evaluation of urinary and reproductive function after inducing protoporphyrin IX with 5-aminolaevulinic acid. *BJU Int* **85**(6):747–753. . PubMed Google Scholar

16. ↵ Kamo I, et al. (2004) The role of bladder-to-urethral reflexes in urinary continence mechanisms in rats. *Am J Physiol Renal Physiol* **287**(3):F434–F441. . Abstract/FREE Full Text Google Scholar

17. ↵ Vogel H (2007) *Drug Discovery and Evaluation: Pharmacological Assays* (Springer, New York), 3rd Ed. . Google Scholar

18. ↵ Johnston GR, Osborne CA, Jessen CR (1985) Effects of urinary bladder distension on the length of the dog and cat urethra. *Am J Vet Res* **46**(2):509–512. . PubMed Google Scholar

19. ↵ Takeda M, Lepor H (1995) Nitric oxide synthase in dog urethra: A histochemical and pharmacological analysis. *Br J Pharmacol* **116**(5):2517–2523. . CrossRef PubMed Google Scholar

20. ↵ Prasad SR, et al. (2005) Cross-sectional imaging of the female urethra: Technique and results. *Radiographics* **25**(3):749–761. . CrossRef PubMed Google Scholar

21. ↵ Kohler TS, Yadven M, Manvar A, Liu N, Monga M (2008) The length of the male urethra. *Int Braz J Urol* **34**(4):451–454, discussion 455–456. . PubMed Google Scholar

22. ↵ Lueders I, Luther I, Scheepers G, van der Horst G (2012) Improved semen collection method for wild felids: Urethral catheterization yields high sperm quality in African lions (*Panthera leo*). *Theriogenology* **78**(3):696–701. . CrossRef PubMed Google Scholar

23. ↵ Balke JM, Boever WJ, Ellersieck MR, Seal US, Smith DA (1988) Anatomy of the reproductive tract of the female African elephant (*Loxodonta africana*) with reference to development of techniques for artificial breeding. *J Reprod Fertil* **84**(2):485–492. . Abstract/FREE Full Text Google Scholar

24. ↵ Hildebrandt TB, et al. (2000) Ultrasonography of the urogenital tract in elephants (*Loxodonta africana* and *Elephas maximus*): An important tool for assessing female reproductive function. *Zoo Biol* **19**(5):321–332. . CrossRef Google Scholar

25. ↵ Fowler ME, Mikota SK (2006) *Biology, Medicine, and Surgery of Elephants* (Wiley-Blackwell, Hoboken, NJ). . Google Scholar

26. ↵ Souza AB, et al. (2008) Comparison of two experimental models of urodynamic evaluation in female rats. *Acta Cir Bras* **23**(Suppl 1):59–65. . PubMed Google Scholar

27. ↵ Russell B, Baumann M, Heidkamp MC, Svanborg A (1996) Morphometry of the aging female rat urethra. *Int Urogynecol J Pelvic Floor Dysfunct* **7**(1):30–36. . CrossRef PubMed Google Scholar

28. ↵ Kunstýř I, Küpper W, Weisser H, Naumann S, Messow C (1982) Urethral plug-a new secondary male sex characteristic in rat and other rodents. *Lab Anim* **16**(2):151–155. . Abstract/FREE Full Text Google Scholar

29. ↵ Root MV, Johnston SD, Johnston GR, Olson PN (1996) The effect of prepuberal and postpuberal gonadectomy on penile extrusion and urethral diameter in the domestic cat. *Vet Radiol Ultrasound* **37**(5):363–366. . CrossRef Google Scholar

30. ↵ Gray H (1918) *Anatomy of the Human Body* (Lea and Febiger, Philadelphia). . Google Scholar

31. ↵ Tsujimoto Y, Nose Y, Ohba K (2003) Experimental and clinical trial of measuring urinary velocity with the pitot tube and a transrectal ultrasound guided video urodynamic system. *Int J Urol* **10**(1):30–35. . CrossRef PubMed Google Scholar

32. ↵ Pozor MA, McDonnell SM (2002) Ultrasonographic measurements of accessory sex glands, ampullae, and urethra of normal stallions of various size types. *Theriogenology* **58**(7):1425–1433. . CrossRef PubMed Google Scholar

33. ↵ Bailey C (1975) Siliceous urinary calculi in bulls, steers, and partial castrates. *Can J Anim Sci* **55**(2):187–191. . CrossRef Google Scholar

34. ↵ Hildebrandt TB, et al. (1998) Reproductive assessment of male elephants (*Loxodonta africana* and *Elephas maximus*) by ultrasonography. *J Zoo Wildl Med* **29**(2):114–128. . PubMed Google Scholar

35. ↵ Walter JS, et al. (2005) Bladder-wall and pelvic-plexus stimulation with model microstimulators: Preliminary observations. *J Rehabil Res Dev* **42**(2):251–260. . CrossRef PubMed Google Scholar

36. ↵ Gutierrez Segura C (1997) Urine flow in childhood: A study of flow chart para Continue on 1,361 uroflowmetry tests. *J Urol* **157**(4):1426–1428. . CrossRef PubMed Google Scholar

37. ↵ Madersbacher S, et al. (1998) The aging lower urinary tract: A comparative urodynamic study of men and women. *Urology* **51**(2):206–212. . CrossRef PubMed Google Scholar

38. ↵ Nitti VW, Tu LM, Gitlin J (1999) Diagnosing bladder outlet obstruction in women. *J Urol* **161**(5):1535–1540. . CrossRef PubMed Google Scholar

39. ↵ Van Asselt E, Groen J, Van Mastrigt R (1995) A comparative study of voiding in rat and guinea pig: Simultaneous measurement of flow rate and pressure. *Am J Physiol* **269**(1 Pt 2):R98–R103. . Google Scholar

40. ↵ Schmidt F, Yoshimura Y, Shin PY, Constantinou CE (2003) Comparative urodynamic patterns of bladder pressure, contractility and urine flow in man and rat during micturition. *APMIS Suppl* **109**(2003):39–44. . PubMed Google Scholar

41. ↵ Masumori N, et al. (1996) Japanese men have smaller prostate volumes but comparable urinary flow rates relative to American men: Results of community based studies in 2 countries. *J Urol* **155**(4):1324–1327. . CrossRef PubMed Google Scholar

42. ↵ Folkestad B, Spångberg A (2004) Timed micturition and maximum urinary flow rate in randomly selected symptom-free males. *Scand J Urol Nephrol* **38**(2):136–142. . CrossRef PubMed Google Scholar

43. ↵ Pandita RK, Fujiwara M, Alm P, Andersson K-E (2000) Cystometric evaluation of bladder function in non-anesthetized mice with and without bladder outlet obstruction. *J Urol* **164**(4):1385–1389. . CrossRef PubMed Google Scholar

44. ↵ Birder LA, et al. (2002) Altered urinary bladder function in mice lacking the vanilloid receptor TRPV1. *Nat Neurosci* **5**(9):856–860. . CrossRef PubMed Google Scholar

45. ↵ Herrera GM, Meredith AL (2010) Diurnal variation in urodynamics of rat. *PLoS ONE* **5**(8):e12298. . CrossRef PubMed Google Scholar

46. ↵ Thor KB, Katofiasc MA (1995) Effects of duloxetine, a combined serotonin and norepinephrine reuptake inhibitor, on central neural control of lower urinary tract function in the chloralose-anesthetized female cat. *J Pharmacol Exp Ther* **274**(2):1014–1024. . Abstract/FREE Full Text Google Scholar

47. ↵ Abdel-Gawad M, Boyer S, Sawan M, Elhilali MM (2001) Reduction of bladder outlet resistance by selective stimulation of the ventral sacral root using high frequency blockade: A chronic study in spinal cord transected dogs. *J Urol* **166**(2):728–733. . CrossRef PubMed Google Scholar

48. ↵ Atalan G, Barr FJ, Holt PE (1998) Estimation of bladder volume using ultrasonographic determination of cross-sectional areas and linear measurements. *Vet Radiol Ultrasound* **39**(5):446–450. . CrossRef PubMed Google Scholar

49. ↵ Higgins AJ, Snyder JR (2006) *The Equine Manual* (Elsevier Saunders, Philadelphia). . Google Scholar

50. ↵ Ishizuka O, et al. (1996) Micturition in conscious rats with and without bladder outlet obstruction: Role of spinal α 1-adrenoceptors. *Br J Pharmacol* **117**(5):962–966. . CrossRef PubMed Google Scholar

51. ↵ Pullan BR, Phillips JI, Hickey DS (1982) Urethral lumen cross-sectional shape: Its radiological determination and relationship to function. *Br J Urol* **54**(4):399–407. . CrossRef PubMed Google Scholar

52. ↵ Fonda D, Hickey DS, Brocklehurst JC (1985) Dynamic shape of the female u… …icturition. Clinical methods. *J Urol* **134**(1):88–91. . PubMed Google Scholar

Continue

53. ↵ Treuting P, Dintzis SM (2011) *Comparative Anatomy and Histology: A Mouse and Human Atlas* (Academic, Waltham, MA). . Google Scholar

54. ↵ Praud C, Sebe P, Mondet F, Sebille A (2003) The striated urethral sphincter in female rats. *Anat Embryol (Berl)* **207**(2):169–175. . CrossRef PubMed Google Scholar

55. ↵ Wheeler AP, Morad S, Buchholz N, Knight MM (2012) The shape of the urine stream—from biophysics to diagnostics. *PLoS ONE* **7**(10):e47133. . CrossRef PubMed Google Scholar

56. ↵ Kim W, Bush JWM (2012) Natural drinking strategies. *J Fluid Mech* **705**:7–25. . CrossRef Google Scholar

57. ↵ Damaser MS, Lehman SL (1995) The effect of urinary bladder shape on its mechanics during filling. *J Biomech* **28**(6):725–732. . CrossRef PubMed Google Scholar

58. ↵ Ghiaasiaan S (2011) *Convective Heat and Mass Transfer* (Cambridge Univ Press, Cambridge, United Kingdom). . Google Scholar

59. ↵ de Gennes P-G, Brochard-Wyart F, Quéré D (2004) *Capillarity and Wetting Phenomena: Drops, Bubbles, Pearls, Waves* (Springer, New York). . Google Scholar

60. ↵ Vogel S (1994) *Life in Moving Fluids: The Physical Biology of Flow* (Princeton Univ Press, Princeton). . Google Scholar

61. ↵ Bush JWM (2010) *18.357 Interfacial Phenomena, Fall 2010*. Available at http://ocw.mit.edu. Accessed May 2, 2014. . Google Scholar

62. ↵ Ogata M, Tomokuni K, Takatsuka Y (1970) Urinary excretion of hippuric acid and *m*- or *p*-methylhippuric acid in the urine of persons exposed to vapours of toluene and *m*- or *p*-xylene as a test of exposure. *Br J Ind Med* **27**(1):43–50. . PubMed Google Scholar

63. ↵ Moore CL, Chadwick-Dias A-M (1986) Behavioral responses of infant rats to maternal licking: Variations with age and sex. *Dev Psychobiol* **19**(5):427–438. . CrossRef PubMed Google Scholar

64. ↵ McMahon TA, Bonner JT, Freeman W (1983) *On Size and Life* (Freeman, New York). . Google Scholar

65. ↵ Schmidt-Nielsen K (1984) *Scaling: Why Is Animal Size So Important?* (Cambridge Univ Press, Cambridge, United Kingdom). . Google Scholar

66. ↵ Dukes H, Reece W (2004) *Dukes' Physiology of Domestic Animals, G - Reference, Information and Interdisciplinary Subjects Series* (Comstock Publishing Associates, Ithaca, NY), 12th Ed. . Google Scholar

67. ↵ Woodburne RT, Lapides J (1972) The ureteral lumen during peristalsis. *Am J Anat* **133**(3):255–258. . CrossRef PubMed Google Scholar

68. ↵ Mortensen NA, Okkels F, Bruus H (2005) Reexamination of Hagen-Poiseuille flow: Shape dependence of the hydraulic resistance in microchannels. *Phys Rev E Stat Nonlin Soft Matter Phys* **71**(5 Pt 2):057301. . CrossRef PubMed Google Scholar

Metabolic theory predicts whole-ecosystem properties
John R. Schramski et al., Proc Natl Acad Sci U S A, 2015

Mosquitoes survive raindrop collisions by virtue of their low mass
Andrew K. Dickerson et al., Proc Natl Acad Sci U S A, 2012

Energetic tradeoffs control the size distribution of aquatic mammals
William Gearty et al., Proc Natl Acad Sci U S A, 2018

Igniting Ca2+ sparks with TRPML1
Gerard P. Sergeant et al., Proc Natl Acad Sci U S A, 2020

A quantitative, theoretical framework for understanding mammalian sleep
Van M. Savage et al., Proc Natl Acad Sci U S A, 2007

X-ray videocystometry for high-speed monitoring of urinary tract function in mice
Jan Franken et al., Sci Adv

Correlation of Urethral Resistance and Shape in Girls
I. Whitaker et al., Radiology, 1968

The role of bladder-to-urethral reflexes in urinary continence mechanisms in rats.
Izumi Kamo et al., American Journal of Physiology - Renal Physiology, 2004

Nonobstructive posterior urethral widening (spinning top urethra) in boys with bladder instability.
H M Saxton et al., Radiology, 1992

Sequential afatinib and osimertinib in patients with EGFR mutation-positive NSCLC and acquired T790M: A global non-interventional study (UpSwinG)
Popat et al., Lung Cancer, 2021

ARTICLE CLASSIFICATIONS

Physical Sciences » Applied Physical Sciences

Biological Sciences » Applied Biological Sciences

Table of Contents

Submit

Sign up for the PNAS *Highlights* newsletter to get in-depth stories of science sent to your inbox twice month:

Enter Email Address

Sign up

Sign up for Article Alerts

Enter Email Address | Sign up

JUMP TO SECTION

Continue

Opinion: How to assess marine cloud brightening's technical feasibility
When it comes to potential geoengineering initiatives, researchers and policymakers need to know what to study—and when to stop.

Image credit: Shutterstock/Venera Salman.

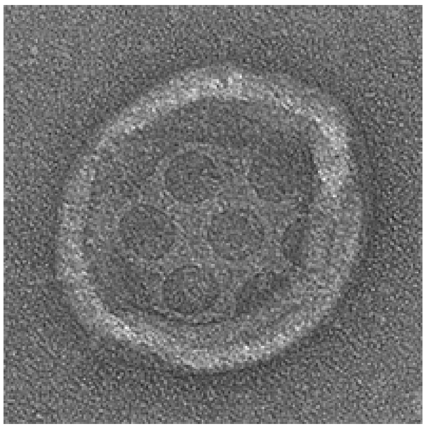

Journal Club: Key immune proteins found in bacteria, not only multicellular life
The gasdermin protein family has unexpectedly ancient origins.

Image credit: Alex Johnson.

Similar Articles

The narrowing of dendrite branches across nodes follows a well-defined scaling law

The allometry of movement predicts the connectivity of communities

Taylor's law of fluctuation scaling for semivariances and higher moments of heavy-tailed data

Scaling of joint mass and metabolism fluctuations in in silico cell-laden spheroids

Energetic scaling in microbial growth

See more